



## Gold(I) selenium *N*-heterocyclic carbene complexes as potent antibacterial agents against multidrug-resistant gram-negative bacteria via inhibiting thioredoxin reductase

Xiuli Chen<sup>a,1</sup>, Shibo Sun<sup>b,1</sup>, Sheng Huang<sup>a,1</sup>, Han Yang<sup>a</sup>, Qing Ye<sup>a</sup>, Lin Lv<sup>a</sup>, Yanshan Liang<sup>a</sup>, Jinjun Shan<sup>c</sup>, Jianqiang Xu<sup>b,\*\*</sup>, Wukun Liu<sup>a,\*</sup>, Tonghui Ma<sup>a,\*\*\*</sup>

<sup>a</sup> School of Medicine & Holistic Integrative Medicine, Nanjing University of Chinese Medicine, Nanjing, 210023, China

<sup>b</sup> School of Life and Pharmaceutical Sciences (LPS) & Panjin Institute of Industrial Technology (PIIT), Dalian University of Technology, Panjin, 124221, China

<sup>c</sup> Medical Metabolomics Center, Nanjing University of Chinese Medicine, Nanjing, 210023, China

### ARTICLE INFO

#### Keywords:

*N*-heterocyclic carbene  
Gold(I) complexes  
Thioredoxin reductase  
Reactive oxygen species  
Drug-resistant bacteria

### ABSTRACT

Multidrug-resistant (MDR) Gram-negative bacteria have become a global threat to human life and health, and novel antibiotics are urgently needed. The thioredoxin (Trx) system can be used as an antibacterial target to combat MDR bacteria. Here, we found that two active gold(I) selenium *N*-heterocyclic carbene complexes **H7** and **H8** show more promising antibacterial effects against MDR bacteria than auranofin. Both **H7** and **H8** irreversibly inhibit the bacterial TrxR activity via targeting the redox-active motif, abolishing the capacity of TrxR to quench reactive oxygen species (ROS) and finally leading to oxidative stress. The increased cellular superoxide radical levels impact a variety of functions necessary for bacterial survival, such as cellular redox balance, cell membrane integrity, amino acid metabolism, and lipid peroxidation. *In vivo* data present much better antibacterial activity of **H7** and **H8** than auranofin, promoting the wound healing and prolonging the survival time of Carbapenem-resistant *Acinetobacter baumannii* (CRAB) induced peritonitis. Most notably in this study, we revealed the influence of gold(I) complexes on both the Trx system and the cellular metabolic states to better understand their killing mechanism and to support further antibacterial drug design.

### 1. Introduction

Antimicrobial resistance is escalating into a profound threat to global public health due to the lack of effective and safe alternative treatments [1]. Carbapenem antibiotics are the last line in defending MDR Gram-negative bacteria infections in the clinical with few other therapeutic options [2]. However, carbapenem-resistant *Enterobacteriaceae* (CRE) has developed resistance to most antibiotics and is associated with high mortality. A study reported in-hospital mortality in 43 (35%) of 123 patients with bloodstream infection of CRE [3,4]. Carbapenem-resistant *Acinetobacter baumannii* (CRAB), carbapenem-resistant *Pseudomonas aeruginosa* (CRPA), carbapenem-resistant *Klebsiella pneumoniae* (CRKP), and carbapenem-resistant *Escherichia coli* (CREco) were placed on the

‘Threat List’ by the World Health Organization (WHO), among which CRAB was listed in the first priority tier, urgently in need of screening and designing novel antibiotics [5]. Hence, it is critical to discover and develop alternative antimicrobial strategies.

Searching for antimicrobial targets that are distinct from conventional antibiotics should be undertaken to reduce the rates of antibacterial resistance [6]. Thioredoxin (Trx) and glutathione (GSH) systems provide antioxidant capacity for Gram-negative bacteria, which play critical roles in maintaining the cellular redox environment [7]. The Trx system contains NADPH, thioredoxin reductase (TrxR) and Trx, which are essential for survival under oxidative stress in some pathogenic bacteria lacking the GSH-Grx system [8,9]. In Gram-negative bacteria, the Trx system not only serves as an antioxidant system but also plays critical roles in DNA replication, redox signaling and cellular protein

\* Corresponding author.

\*\* Corresponding author.

\*\*\* Corresponding author.

E-mail addresses: [jianqiang.xu@dlut.edu.cn](mailto:jianqiang.xu@dlut.edu.cn) (J. Xu), [liuwukun0000@hotmail.com](mailto:liuwukun0000@hotmail.com), [liuwukun0000@njucm.edu.cn](mailto:liuwukun0000@njucm.edu.cn) (W. Liu), [matonghui@njucm.edu.cn](mailto:matonghui@njucm.edu.cn) (T. Ma).

<sup>1</sup> Xiuli Chen; Shibo Sun and Sheng Huang contributed equally to this work.

disulfide/dithiol redox control [8,10]. Thus, the Trx system can be regarded as an important antibacterial target to combat MDR bacteria.

In recent years, gold complexes have attracted attention as promising anticancer agents [11,12], and these complexes exhibit broad-spectrum antimicrobial activity, including against MDR bacteria and fungus [13,14]. Auranofin (AF), a FDA-approved oral gold-containing complex, has a well-studied safety profile with rare, mild, and self-limiting adverse effects. AF has been used in the treatment of rheumatoid arthritis and undergoing Phase II clinical trials for the treatment of amoebic dysentery, giardiasis and tuberculosis. Previous studies showed AF as a potential antimicrobial agent is involving in the inhibition of TrxR, most likely through displacement of two ligands from gold by forming a tight complex between the metal and the active site cysteines of TrxR [15]. Recently, auranofin was identified as an inhibitor of metallo- $\beta$ -lactamases (MBLs) and mobilized colistin resistance, and it resensitized carbapenem- and colistin-resistant bacteria to antibiotics by displacing Zn(II) cofactors from the active site of enzymes involved in antibiotic resistance [16]. Thus, the repurposing of auranofin is a potential therapeutic strategy to overcome drug-resistant bacteria.

Recent studies showed that auranofin has a strong antibacterial effect on Gram-positive bacteria, while it has a weak antibacterial effect on Gram-negative bacteria [15,17]. The weak antibacterial effect of auranofin toward Gram-negative bacteria was suggested to be the result of their glutathione system, glutathione/glutathione reductase, being able to compensate for the loss of reducing capability in the Trx-TrxR system caused by auranofin [18]. Due to the specific metabolism pathway of Gram-negative bacteria, auranofin exhibits relative weak anti-bacteria effects. High dosage of auranofin against Gram-negative bacteria may no longer be adequate. Furthermore, the Au-S bond structure of auranofin is easily attacked by thiols present in the blood and cell membrane, which leads to toxicity and side effects [19]. Therefore, the structural modification of auranofin, which can stabilize gold complexes, has become extremely important.

Selenium (Se), as an analogue of sulfur, has higher reactivity due to the lower  $pK_a$  of selenols than thiols. Meanwhile, Se compounds have attracted a lot of interests recently as promising chemopreventive agents [20]. In addition, *N*-heterocyclic carbenes (NHCs) are a class of ligands whose donor properties form strong coordinate covalent bonds through  $\sigma$  donor properties and  $\pi$ -back-donation to form stable structures [21,22]. Therefore, these ligands play an important role in determining the stability and activity of gold complexes. Based on these results, we substituted the sulfur ligands in the auranofin structure with Se NHC compounds and developed stabilized gold complexes as TrxR inhibitors for MDR bacteria. According to our previous studies on NHC rhodium and gold complexes derived from 4,5-diarylimidazoles, aryl para-substituents and *N* side-chain substituents have certain regularity on the activity of metal complexes [23,24]. What's more, it is well known that phosphine ligands are very important and influential in terms of selectivity for gold complexes. The introduction of Triphenylphosphine (PPh<sub>3</sub>) and Triethylphosphine (PEt<sub>3</sub>) may enhance the lipophilicity and activity of gold complexes [25]. Encouragingly, these complexes show higher antibacterial activity and lower toxicity than auranofin *in vitro* and *in vivo*.

## 2. Materials and methods

### 2.1. Bacterial strains and culture conditions

Auranofin (Yuanye, Shanghai, China) and other gold complexes were dissolved in DMF (Sigma Aldrich, USA). All antibiotics (Yuanye, Shanghai, China) were prepared in sterilized Milli-Q water (Millipore, USA). The CRAB strain was isolated from hospital (High-throughput DNA sequencing results are seen in Fig. S5, Tables S1 and S2). The carbapenem-resistant *Klebsiella pneumoniae* (BAA-1705), carbapenem-resistant *Pseudomonas aeruginosa* (BAA-2108), carbapenem-resistant *Escherichia coli* (BAA-2140), vancomycin-intermediate *Staphylococcus*

*aureus* (ATCC 700699), were purchased from the American Type Culture Collection (Manassas, USA). All the strains were grown in Luria-Bertani (LB) broth containing 10 g/L tryptone (Aobox, Beijing, China), 5 g/L yeast extract (AOBOX, Beijing, China) and 10 g/L NaCl (Solarbio, Beijing, China).

### 2.2. Chemicals

General synthesis of gold complexes **H1–H17** is presented in Fig. 1 and in detail in the Supplementary Material.

### 2.3. Stability analysis of **H7** and **H8**

Complex **H7**, **H8** was accurately weighed and dissolved in DMF to prepare 20 mM solution, and then diluted to 0.4  $\mu$ M solution with PBS (10 mM, pH = 7.2). A UV-Vis spectrophotometer was used to scan the full UV wavelength of diluent for 0 h, 6 h, 12 h, 24 h, 48 h, 72 h, 120 h and 168 h successively, and observe the UV absorption changes at 298 K over 7 days.

### 2.4. Solubility of compounds

Measure the maximum absorption wavelength of **H7** in PBS: DMF = 500: 1 with a UV-Vis spectrophotometer at 298 K. To obtain a stock solution, **H7** was weighed and dissolved in DMF, then add 500 times (v/v) PBS and mix well. The stock solution was then diluted with PBS: DMF = 500: 1, made into solutions of various concentrations, and their UV absorbance values at 236 nm were measured sequentially, followed by the drawn of a standard curve (Fig. S14). In the same approach, a saturated solution of **H7** was made, the upper clear solution was taken after centrifugation and diluted four times. Then the absorbance at 236 nm was measured to calculate the solubility of **H7**.

### 2.5. Genome sequencing of CRAB

Genomic DNA was extracted with the SDS method. The harvested DNA was detected by the agarose gel electrophoresis and quantified by Qubit 2.0 Fluorometer (Thermo Fisher Scientific, USA).

A total amount of 1  $\mu$ g DNA per sample was used as input material for the DNA sample preparations. Sequencing libraries were generated using NEBNext® Ultra™ DNA Library Prep Kit for Illumina (NEB, USA) following manufacturer's recommendations and index codes were added to attribute sequences to each sample. Briefly, the DNA sample was fragmented by sonication to a size of 350 bp, then DNA fragments were end-polished, a tailed, and ligated with the full-length adaptor for Illumina sequencing with further PCR amplification. At last, PCR products were purified (AMPure XP system) and libraries were analyzed for size distribution by Agilent 2100 Bioanalyzer and quantified using real-time PCR.

The whole genome of CRAB was sequenced using Illumina NovaSeq PE150 at the Beijing Novogene Bioinformatics Technology Co., Ltd.

### 2.6. Screening of antibacterial activity of gold complexes and ligands

Antibacterial effect of gold complexes (**H1–H17**) and the synthesized ligands (**S1–S9**) were determined by microbroth dilution method referring to CLSI guidelines as described previously [26]. 96-well plates were incubated at 37 °C in the incubator (Thermo Fisher Scientific, Waltham, USA) and measured manually following 24 h of incubation by microplate reader (PerkinElmer, USA).

### 2.7. Cytotoxicity assays

Cell Counting kit-8 (CCK-8) allows convenient assays using WST-8[2-(2-methoxy-4-nitrophenyl)-3-(4-nitrophenyl)-5-(2,4-disulfophenyl)-2H-tetrazolium, monosodium salt], which produces a water-soluble

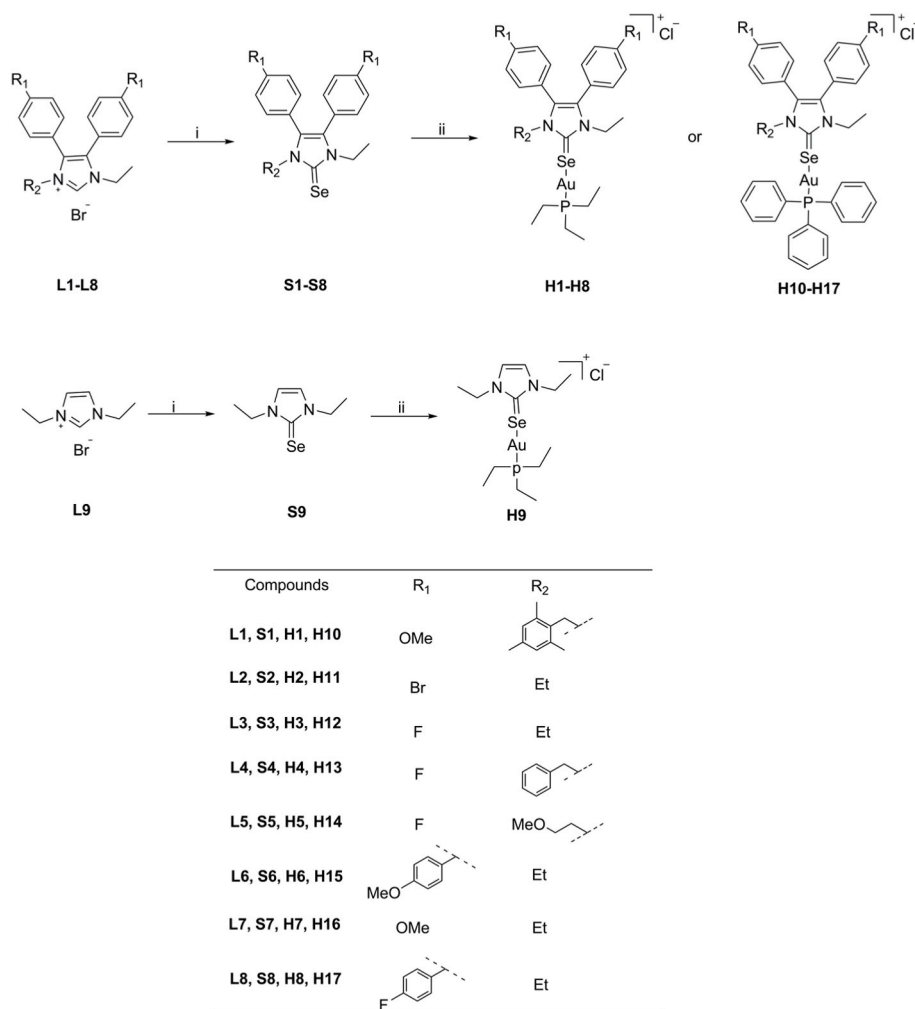


**Fig. 1.** The synthetic route and chemical structures of **H1–H17**: i: Se, KOtBu, THF, 0 °C, 5 h; ii: Et<sub>3</sub>PAuCl/Ph<sub>3</sub>PAuCl, DCM, Ar, rt, darkness, 20 min.

formazan dye upon reduction in the presence of an electron carrier, 1-Methoxy PMS. CCK-8, being nonradioactive, allows sensitive colorimetric assays for the determination of the number of viable cells in cell proliferation and cytotoxicity assays. The cell survival rate of target gold complexes were determined by the CCK-8 assay kit (Solarbio, Beijing, China) as described previously [27]. Briefly, before being treated, cells (Vero and LO<sub>2</sub>) were seeded in 96-well plates for 24 h, and cells were exposed to gold complexes at different concentrations (0, 1, 2, 5, 10 μM) for 72 h. Then, supernatant was removed from the 96-well plates and CCK-8 solution was added into each well. The cytotoxicity of was measured at OD<sub>570nm</sub> after being incubated for 4 h at 37 °C.

## 2.8. Screening of synergistic effect of antibiotic with gold complexes

Screening of synergistic effect of antibiotic with gold complexes (**H7**, **H8** and auranofin) by using checkerboard microdilution assay as previous described [16]. Briefly, the bacterial suspension was diluted according to CLSI microbroth dilution method, and seeded in each well of 96-well plate. Then, the bacterial suspension was exposed to the treatment of gold complexes at different concentrations (0–20 μM) in the presence of different antibiotic concentrations (0–240 μM). The inhibition rate was measured by microplate reader at OD<sub>600nm</sub>.

## 2.9. Intracellular gold uptake

Bacteria culture was diluted to OD<sub>600nm</sub> of 0.4–0.6, and treated with **H7**, **H8** or auranofin (20 μM) for 2 h. Cells were collected and washed

twice with ice-cold PBS, and normalized to OD<sub>600nm</sub> of 0.5 ± 0.02. Then, 1 mL bacterial culture of each sample was collected for further measurement. Cell pellets were collected after centrifugation and digested with HCl (0.5 mL), followed by the addition of 4.5 mL of ddH<sub>2</sub>O<sub>2</sub> and the final gold content was determined by Thermo X series 2 ICP-MS (Thermo, USA).

## 2.10. Cellular activities of TrxR assay

TrxR catalyzes NADPH to reduce 5,5'-Dithiobis-(2-nitrobenzoic acid) (DTNB) to form TNB and NADP<sup>+</sup>, TNB has a absorbance at 412 nm, but reduced glutathione reacts with DTNB to form TNB, so the 2-Vinylpyridine in this kit can inhibit reduced glutathione in sample, the activity of TrxR can be calculated by detecting the increase rate of TNB at 412 nm. The activity of cellular TrxR was determined according to the TrxR activity detection kit (Solarbio, Beijing, China). Briefly, bacteria culture was diluted to OD<sub>600nm</sub> of 0.4–0.6, and treated with different concentrations (0, 0.5, 1, 2, 5, 10, 20 μM) of gold complexes (**H7**, **H8**, auranofin) for 2 h. The cell pellets were harvested and washed with PBS for three times. Bacterial cells were normalized to OD<sub>600nm</sub> of 0.7 ± 0.02. The cellular TrxR was measured by the microplate reader followed the protocol of TrxR Assay Kit.

## 2.11. Inhibition of purified selenoprotein TrxR

Inhibition to the activity of purified TrxR (purified rat liver TrxR was purchased from Sigma Aldrich) by **H7** and **H8** were determined

according to previously method [28].

### 2.12. Expression of CRAB TrxR in *E. coli*

DNA sequence (957 bp) containing TrxR (encoded by *trxR*, 315 aa) from CRAB was synthesized by Sangon Biotech. Co. (Shanghai, China) and then constructed into a pET-28a vector with an N-terminal 6 × His tag by subcloning a *Nco*I/*Bam*H I fragment. Recombinant CRAB TrxR with an N-terminal 6 × His tag was produced in *Escherichia coli* (*E. coli*). In brief, *E. coli* BL21 cells were transformed with the plasmid containing CRAB TrxR gene and a single colony was grown in LB medium at 37 °C with 200 rpm overnight. Next day, the cultured cells were inoculated into fresh medium and cultured for 1.5–2.0 h ( $OD_{600nm} = 0.5$ ). Then, 0.5 mM IPTG was added in the medium and the induced expression was performed at 24 °C with 200 rpm for additional 24 h. Bacterial cells were centrifuged and wet pellets were harvested, and used for further separation and purification.

### 2.13. Purification of recombinant CRAB TrxR

The harvested bacterial pellets were suspended in a binding buffer (50 mM Tris, 150 mM NaCl and 20 mM imidazole) and lysed by freeze-thawing three times with 1 mg/mL lysozyme and ultrasonicator in ice. After centrifugation at 18,000 rpm for 30 min, the supernatant fraction was subject to a prepacked nickel column (HisTrap FF crude, Cytiva, USA) and then loaded to a gel filtration column (HiPrep Sepharacryl S-200, Cytiva, USA) after being concentrated by a 30 kDa cut-off ultrafiltration device (50 mL spin column, Millipore, USA) (Fig. S11). The protein concentration of CRAB TrxR was determined by measuring FAD absorbance at 463 nm with the extinction coefficient of  $11,300 M^{-1} cm^{-1}$  as previously described [29,30].

### 2.14. Enzymatic activity of CRAB TrxR

Activity of CRAB TrxR was determined by using a standard DTNB-reducing activity assay as described in previous reports [31,32]. The working reaction mixture contains 100 nM CRAB TrxR (dimeric form), 2.5 mM DTNB, 300 μM NADPH in a TE buffer (pH 7.5). TrxR-mediated DTNB reduction was evaluated by the formation of TNB<sup>-</sup> following the initial slope @ A412 nm for 3 min, with the extinction coefficient of 13,600  $M^{-1} cm^{-1}$ . The kinetic parameters were determined using a varied DTNB concentrations in range from 0 to 5 mM and fitted into Michaelis-Menten equation by Prism 8.0 (GraphPad, USA).

### 2.15. Inhibition of CRAB TrxR by gold complexes

2 μM CRAB TrxR was pre-reduced by 100 μM NADPH for 10 min at room temperature ( $22 \pm 1$  °C) to reduce the redox-active disulfide bond. NADPH-reduced TrxR was then treated with auranofin, **H7** and **H8** as indicated. The residual TrxR activity was determined by DTNB reducing assay.

### 2.16. Quantitative real-Time PCR

The IC<sub>50</sub> value concentrations of gold complexes (**H7**, **H8**) were established with the initial  $OD_{600nm}$  of 0.4–0.5 and shaken for 2 h at 37 °C. Total RNA were extracted from the bacterial cells according to the Total RNA Extraction Kit (Solarbio, Beijing, China) protocol. Briefly, adding 1 mL lysis buffer to lyse cells directly, after incubate homogenized samples at room temperature for 5 min, per 1 mL lysis buffer was added 200 μL of chloroform for homogenization. Then centrifuge the sample, pipette the aqueous phase out into a new tube. Preparation RNase free collection column, and add 200 μL ethanol in the aqueous phase and vortex, transfer the aqueous phase in the collection column. Then add the washing buffer in collection column tube twice to wash the column, and place the RNase-free spin column in a new 1.5 mL

collection tube to elute the RNA. The quality of RNA was detected by electrophoresis. Hifair ®II 1st Strand cDNA Synthesis Kit (Tiangen, Beijing, China) was applied to reverse transcription. The cDNA was then used in the real-time qPCR experiment using the SYBR Green qPCR Master Mix (Bimake, Houston, USA) with the QuantStudio™ 6 Flex Real-Time PCR system (Thermo Fisher Scientific, MA, USA). All assays were performed in triplicate. 16s was used as an internal control gene. Relative expression was calculated by using the  $2^{-\Delta\Delta Ct}$  method. The following primers for qPCR were used:

16s (forward): 5'-CAGC-TCGT-GTCG-TGAG-ATGT-3'

16s (reverse): 5'-CGTA-AGGG-CCAT-GATG-ACTT-3'

TrxB (forward): 5'-ACGA-AAGA-TGAC-AGCA-AACA-AG-3'

TrxB (reverse): 5'-AGCC-ATAC-AGCC-TGAA-CCC-3'

### 2.17. Measurement of intracellular superoxide radical

Dihydroethidium (DHE) probe is one of the most used fluorescent probes for detecting superoxide radical, which can be oxidized to form ethyl oxide by intracellular ROS, producing red fluorescence through incorporation into chromosomal DNA. The intensity of red fluorescence is proportional to the level of ROS in cells. Bacteria culture was diluted to  $OD_{600nm}$  of 0.4–0.5 and incubated with DHE probe at 37 °C and shaken for 20 min. Then, the cell culture was incubated with gold complexes (auranofin, **H7** and **H8**) of different concentrations (0, 10, 20, 40, and 80 μM) for 30 min, respectively. Cells were collected and washed twice with PBS, and each sample was then resuspended in 1 mL PBS for measurement. All the data was collected using BD Accuri™ C6 Plus flow cytometry with a 480–535 nm argon laser and a 590–610 nm emission filter at low flow rate. At least 100,000 cells were collected for each sample. FlowJo V10 was used for processing flow cytometric data.

### 2.18. Membrane permeabilization assay

Propidium iodide (PI) uptake assay was used to determine the membrane permeability of auranofin, **H7** and **H8** by cytometry method as previously described. In brief, bacteria culture was diluted to  $OD_{600nm}$  of 0.4–0.5 and incubated with PI (50 μg/mL) shaken for 20 min at 37 °C. Then, the cell culture was incubated with gold complexes (auranofin, **H7** and **H8**) at different concentrations (0, 10, 20, 40, 80 μM) for 30 min, respectively. Cells were collected and washed twice with PBS, and each sample was then resuspended in 1 mL PBS for measurement. All the data were collected using BD Accuri™ C6 Plus flow cytometry with a 480–535 nm argon laser and a 590–610 nm emission filter at low flow rate. At least 100,000 cells were collected for each sample. FlowJo V10 was used for processing flow cytometric data.

### 2.19. Preparation of intracellular metabolites extracts

Preparation of cellular metabolite extracts was carried out as previously described [33]. In brief, bacterial pellets were collected after being treated with **H7**, **H8** (20 μM) at 2 h and resuspended in 600 μL methanol: water mixture (9: 1, v/v) at –80 °C, containing 1,2-<sup>13</sup>C myristic acid (internal standard). Three freeze-thaw cycles in liquid nitrogen were used for lysing cells and releasing cellular metabolites, which followed by ultrasonic cell crusher (Scientz, Ningbo, China) to disrupt each sample for 10 min. Then, all the samples were centrifuged at 8000 g for 10 min at 4 °C. 450 μL of supernatant was collected for derivatization and metabolomics analysis described previously [34].

### 2.20. Measurement of cellular GSH

The reduced form of glutathione (GSH) is a natural tripeptide composed of glutamic acid (Glu), cysteine (Cys) and glycine (Gly). Glutathione can react with DTNB to produce 2-nitro-5-mercaptobenzoic acid and glutathione disulphide (GSSG). 2-nitro-5-mercaptobenzoic acid is a yellow product with the maximum absorption at 412 nm. Bacteria

were treated with **H7** (0, 10, 20, 40  $\mu\text{M}$ ) and **H8** (0, 10, 20, 40  $\mu\text{M}$ ), respectively and then continued to culture at 200 rpm for 2 h at 37  $^{\circ}\text{C}$ . After centrifugation at 4000 g for 15 min at 4  $^{\circ}\text{C}$  to harvest bacterial cells, cell pellets were washed for three times with PBS. Bacterial cells were normalized to  $\text{OD}_{600\text{nm}} = 0.70 \pm 0.02$  and subsequently disrupted using ultrasonic cell crusher for 10 min to lyse cells. After centrifugation at 8000 g for 10 min at 4  $^{\circ}\text{C}$ , the supernatant was collected for cellular GSH measurement. The cellular GSH level was measured by the Reduced Glutathione Content Assay Kit (Solarbio, Shanghai, China), using the microplate reader (PerkinElmer, USA).

#### 2.21. Determination of intracellular $\text{K}^+$ , $\text{Mg}^{2+}$ , MDA, and SOD

Bacteria were treated separately with **H7** (0, 10, 20, 40  $\mu\text{M}$ ) and **H8** (0, 10, 20, 40  $\mu\text{M}$ ), and shaken at 200 rpm for 2 h at 37  $^{\circ}\text{C}$ . After centrifugation at 4000 g for 15 min at 4  $^{\circ}\text{C}$ , cell pellets were washed for three times with PBS. Bacterial cells were normalized to  $\text{OD}_{600\text{nm}} = 0.70 \pm 0.02$ , and then the internal  $\text{K}^+$ ,  $\text{Mg}^{2+}$ , malondialdehyde (MDA), and superoxide dismutase (SOD) were determined according to the protocols of  $\text{K}^+$ ,  $\text{Mg}^{2+}$ , MDA and SOD activity assay kits (Jiancheng, Nanjing, China).

#### 2.22. Determination of DNA degradation

Genomic DNA from CRAB was collected by using the MiniBEST Bacteria Genomic DNA Extraction Kit ver.3.0 (TaKaRa, Japan). The DNA was then treated with different concentrations (0, 5, 10, 20, 40  $\mu\text{M}$ ) of **H7** and **H8** for 2 h, respectively. Finally, DNA degradation was determined by using the agarose gel electrophoresis with ethidium bromide (EB) staining and documented by using Gel imaging system (Tanon, China).

#### 2.23. Animal approval

All BALB/c mice (No.SYXK-2018-0049) were domesticated under standard laboratory conditions and were given free access to standard water and food. All procedures were approved by the Laboratory Animal Ethics Committee of Nanjing University of Chinese Medicine.

#### 2.24. Murine skin wound infection model

Twenty male BALB/c (18–22 g) mice were randomly divided into 7 groups ( $n = 4$ ), and 200  $\mu\text{L}$   $1 \times 10^9$  CFU of CRAB was inoculated on the back skin wounds of mice. The mice were then treated with 30  $\mu\text{L}$  0.9% NaCl,  $\text{H}_2\text{O}_2$  (5 mM), auranofin (5 mM), imipenem (5 mM), colistin (5 mM), **H7** (5 mM) or **H8** (5 mM) once per day for 14 days, respectively. Twenty-four hours after the last treatment, the skin of the wound was excised for inflammatory cytokines, pathological and IHC detection. The wound healing was calculated by formula as follows:  $F = (\text{A}-\text{B})/\text{A} \times 100\%$ , where F: wound healing rate, A: original wound area, and B: wound area post-treatment. This animal experiment was repeated three times.

#### 2.25. Murine peritonitis infection model

Thirty-two male BALB/c (18–22 g) mice were randomly divided into 4 groups ( $n = 8$ ), and forty-eight female BALB/c (18–22 g) mice were randomly divided into 4 groups ( $n = 12$ ). Then, the BALB/c mice were infected i.p. with 200  $\mu\text{L}$   $10^9$  CFU of CRAB. After 1h infection, the mice in the four groups were i.p. injected with PBS, auranofin (5 mg/kg), **H7** (5 mg/kg) and **H8** (5 mg/kg) respectively. The survival rate within 72 h was observed. This animal experiment was repeated three times.

#### 2.26. Statistical analysis

GraphPad Prism 7.0 software was used for statistical analysis.

Student's t-test was performed for determination of differences between groups and statistical significance was considered at value of  $p < 0.05$ .

### 3. Results and discussion

#### 3.1. Synthesis and characterization of gold complexes

The synthetic routes of gold(I) selenium NHC complexes **H1–H17** are outlined in Fig. 1. The diarylimidazolium salts **L1–L9** and Se–NHC compounds (**S1–S9**) were prepared according to our previously published methods [35]. Initially, the ligands (**L1–L9**), Se powder and potassium *tert*-butoxide (KOtBu) were dissolved in tetrahydrofuran (THF) in an ice bath to obtain Se–NHC compounds (**S1–S9**). Then, Se–NHC compounds (**S1–S9**) and gold complexes chloro (triphenylphosphine) gold(I) or chloro (triethylphosphine) gold(I) were stirred at room temperature for 20 min in the dark under the protection of argon to obtain complexes **H1–H17** (Fig. 1). The gold complexes were characterized by  $^1\text{H}$  NMR,  $^{13}\text{C}$  NMR and MS spectra. Except for the newly generated peaks of  $\text{PPh}_3$  and  $\text{PEt}_3$  in **H1–H17**, there is no obvious change in the chemical shift of the  $^1\text{H}$  NMR and  $^{13}\text{C}$  NMR spectra between the selenium compounds **S1–S9** and gold complexes **H1–H17**, which might be due to the weak coordination of the gold atom with selenium atom. From the ESI mass spectra, we can observe the peaks of  $[\text{M} - \text{Cl}]^+$  for gold complexes **H1–H17**. In addition, the purity of all complexes was higher than 95% (m/m) as determined by elemental analysis or HPLC. The stability of representative complexes **H7** and **H17** in water solution was tested over 7 days by examining the  $^1\text{H}$  NMR spectra of complexes **H7** and **H17** (Figs. S1 and S3). The  $^1\text{H}$  NMR spectra of complexes **H7** and **H17** did not change significantly within 7 days, indicating that complexes **H7** and **H17** were very stable in DMSO- $d_6$ /D $_2$ O (9/1) solution. The stability of the main complexes **H7** and **H8** in PBS (10 mM, pH = 7.2), which is similar with *in vitro*/*in vivo* studies, was investigated using a UV spectrophotometer. As shown in Figs. S2 and S4, the UV absorption spectra of **H7** and **H8** did not change considerably during 7 days, demonstrating that complexes **H7** and **H8** were relatively stable in PBS.

#### 3.2. Antibacterial activities of gold complexes and ligands

We firstly evaluated the antibacterial activity of synthesized ligands (**L1–L9**) and their gold(I) complexes (**H1–H17**). The measurements were performed on MDR bacteria (CRAB, CRKP, CRPA and CREco) and vancomycin-intermediate *Staphylococcus aureus* (VISA), among which CRAB was isolated from a hospital (the high-throughput DNA sequencing results are shown in Fig. S5 and Tables S1 and S2; NCBI accession code JAKLSN000000000). We also tested the antibiotic sensitivity of CRAB (Table S3) and results showed that the CRAB had developed resistance to most antibiotics. These strains were chosen because they represent pathogens urgently needing research and the development of novel antibiotics.

The MIC values of all complexes are shown in Table 1. Among the 17 complexes, **H7** and **H8** showed quite strong antibacterial activity against the MDR bacteria (MIC values of 10–20  $\mu\text{M}$ ) and VISA (MIC values of 0.2  $\mu\text{M}$ ), which was generally better than the MIC values of auranofin. All of the other complexes showed no activity (CRKP, CRPA and CREco) up to 40  $\mu\text{M}$ . The synthesized ligands (**L1–L9**) showed no activity (Table S4), which indicated that their antibacterial activities were primarily dependent on the presence of gold.

As the gold complexes displayed potential cytotoxicity, we next measured the cytotoxicity of the two gold(I) complexes (**H7** and **H8**) in comparison to auranofin against two normal cell lines (Vero and LO $_2$ ). The complexes **H7** and **H8** displayed a similar or even lower cytotoxicity in comparison to auranofin (Fig. S6). Additionally, to estimate the bioavailability of these complexes, we found that the solubility of **H7** is about 310  $\mu\text{g}/\text{mL}$  under conditions similar to the culture medium (PBS: DMF = 500: 1, v/v) through experiment (Fig. S10). Therefore, **H7** and **H8** are better antibacterial agent choices than auranofin and deserved a

**Table 1**  
The minimum inhibitory concentration (MIC) of gold complexes against MDR bacteria.

Complexes	CRAB		CRKP		CRPA		CREco		VISA	
	$\mu\text{M}$	$\mu\text{g/mL}$								
H1	10	8.71	>40	>34.84	>40	>34.84	>40	>34.84	0.2	0.17
H2	10	8.64	40	34.56	>40	>34.56	>40	>34.56	2	1.73
H3	10	7.42	40	29.68	>40	>29.68	>40	>29.68	2	1.48
H4	10	8.04	40	32.16	>40	>32.16	>40	>32.16	2	1.61
H5	10	7.72	40	30.88	>40	>30.88	>40	>30.88	2	1.54
H6	>40	>36.72	>40	>36.72	>40	>36.72	>40	>36.72	>40	>36.72
H7	10	7.66	20	15.32	20	15.32	20	15.32	0.2	0.15
H8	10	8.94	20	17.88	20	17.88	20	17.88	0.2	0.19
H9	20	11.08	40	22.16	>40	>22.16	>40	>22.16	5	2.77
H10	40	>40.56	>40	>40.56	>40	>40.56	>40	>40.56	5	5.07
H11	>40	>40.32	>40	>40.32	>40	>40.32	>40	>40.32	5	5.04
H12	>40	>35.44	>40	>35.44	>40	>35.44	>40	>35.44	5	4.43
H13	>40	>37.92	40	37.92	40	37.92	>40	>37.92	1	0.95
H14	>40	>36.64	>40	>36.64	>40	>36.64	>40	>36.64	40	36.64
H15	>40	>42.48	>40	>42.48	>40	>42.48	>40	>42.48	5	5.31
H16	20	18.20	>40	>36.40	>40	>36.40	>40	>36.40	5	4.55
H17	>40	>41.52	>40	>41.45	>40	>41.45	>40	>41.45	10	10.38
Auranofin	20	13.56	40	27.12	40	27.12	40	27.12	0.5	0.34

further study.

To gain insights into the potential targets of **H7** and **H8**, we used CRAB as a model for further investigation. First, we used a whole-cell uptake assay to measure the uptake of gold into the cell to investigate the relationship between the content of cellular gold and antibacterial efficacy. Whole-cell uptake was measured in  $\sim 100$  million cells after 2 h of treatment with 20  $\mu\text{M}$  gold complexes (auranofin, **H7** and **H8**). The results showed that the uptake of **H7** (45.11 ng/g protein) and **H8** (53.42 ng/g protein) was higher than that of auranofin (16.64 ng/g protein) (Fig. 2). Then, we measured the gold uptake at 20, 40, 80, 100, 120 min of treatment with 20  $\mu\text{M}$  gold complex (**H8**). The results showed that the intracellular gold content gradually increased from 20 min to longer time and reached the peak at 80 min (Fig. S7). The decrease of gold content after 80 min may be caused by cell membrane rupture leading to gold escape. This result provides a better correlation between gold cellular uptake and antibacterial activity.

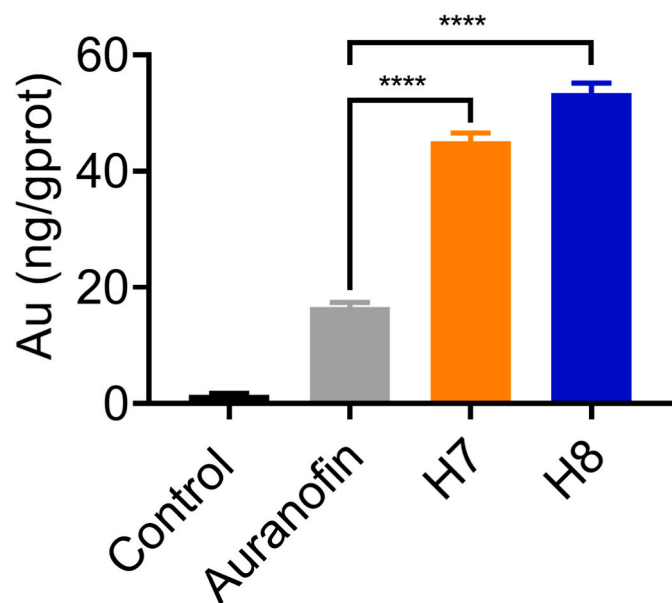


**Fig. 2.** Whole-cell uptake of 20  $\mu\text{M}$  gold complexes (auranofin, **H7** and **H8**) by CRAB after 2-h treatment. Statistical significance of the differences in mean values are \*\*\*\* $p < 0.0001$ . (For interpretation of the references to color in this figure legend, the reader is referred to the Web version of this article.)

### 3.3. Synergistic antibacterial action

Design and screening of novel agents for decreasing bacterial resistance through combinations of antibacterial therapeutics have attracted numerous attentions [36]. Next, we screened the antimicrobial activity of antibiotics (such as  $\beta$ -lactam antibiotics (ampicillin, cefotaxime, imipenem), quinolones (norfloxacin) and aminoglycosides (gentamicin) and the gold complexes (auranofin, **H7** and **H8**). As shown in Fig. 3 and Fig. S8, the combination of auranofin with cefotaxime and imipenem led to additive killing of CRAB with fractional inhibitory concentration index (FICI) ranging from 0.56 to 0.75. The MIC value of cefotaxime decreased from 240  $\mu\text{M}$  to 30  $\mu\text{M}$  in the presence of **H7**, **H8** (2.5  $\mu\text{M}$ ), for which the FICI was estimated to be 0.375 (Table 2), i.e., indicative of synergy (FICI  $\leq 0.5$ ). The combination of **H7** and **H8** with imipenem showed synergistic killing of CRAB with an FICI of 0.5. Thus, our combined data clearly demonstrated that the combined effect of **H7** and **H8** with cefotaxime and imipenem was stronger than that of auranofin.

### 3.4. The affinity of complexes to TrxR

The thioredoxin system, including TrxR, plays an important role in controlling cellular redox balance and signaling [10]. In Gram-positive bacteria such as *Staphylococcus aureus*, the gold center of auranofin could inhibit the activity of TrxR, triggering cellular ROS production [15]. Previous studies shown that auranofin, ebselen, shikonin, and alicin exert antibacterial activity against Gram-positive bacteria by inhibiting TrxR, which indicated that TrxR may be a potential antimicrobial target and provide new ideas for the development of antibacterial drugs [37]. However, most Gram-negative bacteria possess an additional GSH system, which helps to defend against auranofin by destroying the stability of the complex.

Therefore, we substituted the sulfur ligands in the auranofin structure with selenium NHC to develop gold complexes with a stronger TrxR inhibitory effect. To demonstrate this hypothesis, we explored the TrxR inhibitory effect of auranofin, **H7** and **H8** in CRAB. TrxR assay kits were used to determine the inhibitory effect of TrxR activity with different concentrations of gold complexes (auranofin, **H7** and **H8**). Auranofin potently inhibited CRAB TrxR enzymes in a dose-dependent manner ( $\text{IC}_{50} = 6.31 \mu\text{M}$ ), and the enzyme inhibitory activities of **H7** and **H8** were higher than that of auranofin (**H7**  $\text{IC}_{50} = 1.58 \mu\text{M}$ ; **H8**  $\text{IC}_{50} = 1.20 \mu\text{M}$ ) (Fig. 4a–c). In addition, we tested the TrxR inhibitory activity of **H7** and **H8** against an isolated enzyme. As demonstrated in Fig. S9, purified TrxR activity was substantially and dose-dependently inhibited by **H7** ( $\text{IC}_{50} = 14.69 \text{ nM}$ ) and **H8** ( $\text{IC}_{50} = 16.64 \text{ nM}$ ), which were much more

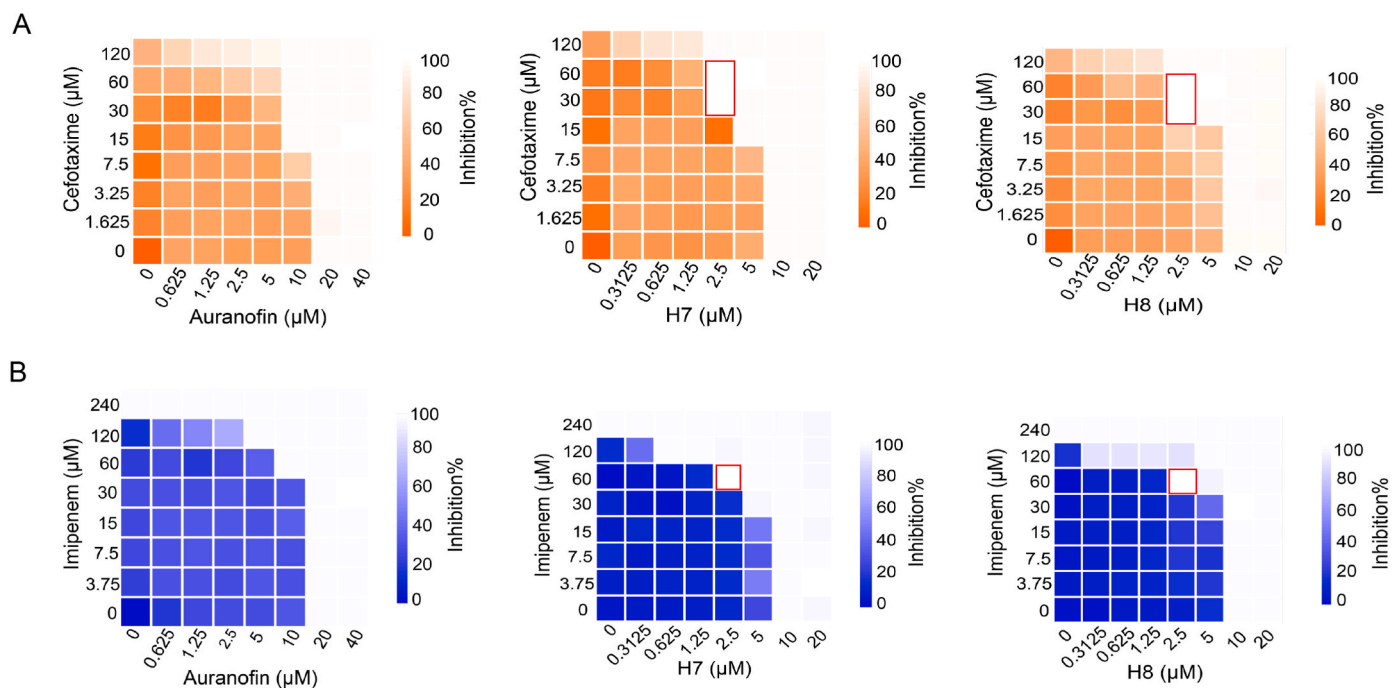


**Fig. 3.** Heat plots of microdilution checkerboard assays for the combination of cefotaxime (A), imipenem (B) and auranofin and H7 and H8 against CRAB. The red box in Fig. 3 is synergistic regions. (For interpretation of the references to color in this figure legend, the reader is referred to the Web version of this article.)

**Table 2**

Potency of gold complexes (auranofin, H7 and H8) in combination with different classes of antibiotics against CRAB.

Antibiotic	MIC ( $\mu\text{M}$ )	FIC index (H7)	FIC index (H8)	FIC index (auranofin)
Cefotaxime	240	0.375	0.375	0.625
Imipenem	240	0.5	0.5	0.75

potent than that of auranofin in our previous report ( $\text{IC}_{50} = 82.6 \text{ nM}$ ) [38]. In CRAB, thioredoxin reductase (TrxR) is encoded by *TrxB* (Gene ID: 66398184). We subsequently examined the relationship between

TrxB expression levels and H7, H8 and auranofin treatment in CRAB by qPCR. The result showed that the expression of TrxB was decreased by H7 ( $p < 0.5$ ), however, the decrease of TrxR at mRNA level is minor comparing to the remarkable inhibition of the TrxR activity after H7 treatment, and auranofin and H8 had no effect on expression of TrxB (Fig. S10), which further confirmed that the anti-CRAB activity of H7 and H8 compounds is caused by the direct inhibition on CRAB TrxR, rather than the regulation of the mRNA levels of TrxR.

To further confirm the inhibition of CRAB TrxR by gold complexes (auranofin, H7 and H8), we recombinantly expressed the CRAB TrxR in *E. coli* and then purified the enzyme using nickel affinity chromatography and gel filtration chromatography (Fig. S11). The collected

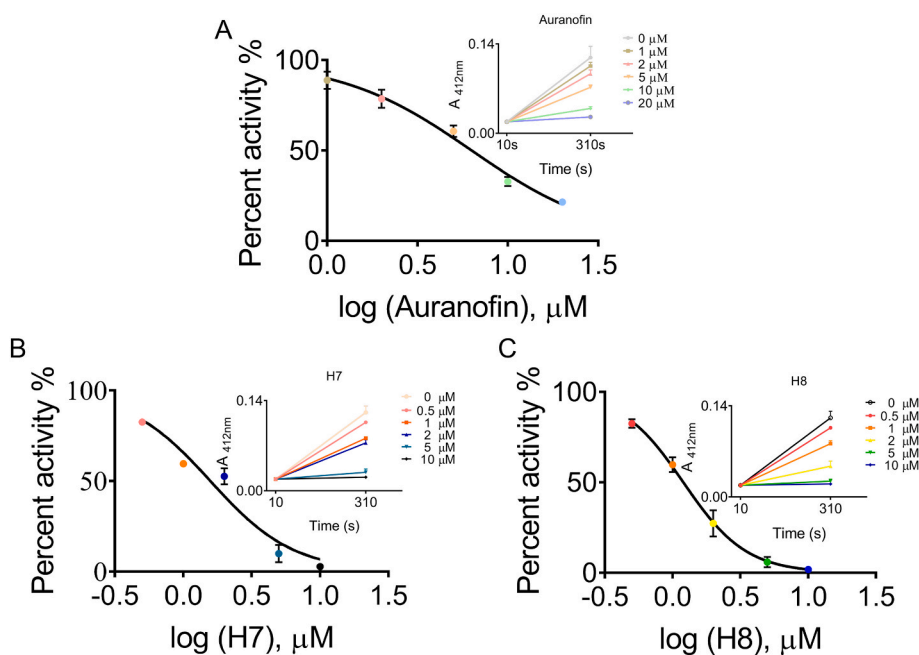


**Fig. 4.** H7 and H8 exhibit higher TrxR affinity. (A–C) Inhibition of the activity of TrxR in CRAB. The auranofin concentrations tested were 20, 10, 5, 2, and 1  $\mu\text{M}$ ; the H7 concentrations tested were 10, 5, 2, 1, and 0.5  $\mu\text{M}$ ; and the H8 concentrations tested were 10, 5, 2, 1, and 0.5  $\mu\text{M}$ . Dose-response plots of CRAB TrxR activity with and without a 2 h pre-incubation with different concentrations of gold complexes. (For interpretation of the references to color in this figure legend, the reader is referred to the Web version of this article.)

fractions were analyzed by using a reducing SDS-PAGE, and the CRAB TrxR is observed at the low molecular weight (36 kDa) in the gel (Fig. 5A). We then determined the kinetic parameters of CRAB TrxR using a standard DTNB-reducing activity assay. In this assay, reaction progress was monitored by measuring the absorbance of the liberated TNB chromophore at 412 nm. Under these conditions, we obtained a  $K_M$  value of 7.3 mM for recombinant CRAB TrxR (Fig. 5B). When

preincubated with TrxR and NADPH, we found that gold complexes rapidly inhibited the enzyme in a dose-dependent manner, with  $IC_{50}$  values of 9.76  $\mu M$  of auranofin, and the enzyme inhibitory activities of H7 and H8 were higher than that of auranofin (H7  $IC_{50} = 4.75 \mu M$ ; H8  $IC_{50} = 5.08 \mu M$ ) (Fig. 5C) (Fig. S12B). Furthermore, we determine the activities of the desalted and unsalted enzymes, and the results showed that recombinant CRAB TrxR were irreversibly inhibited by H7

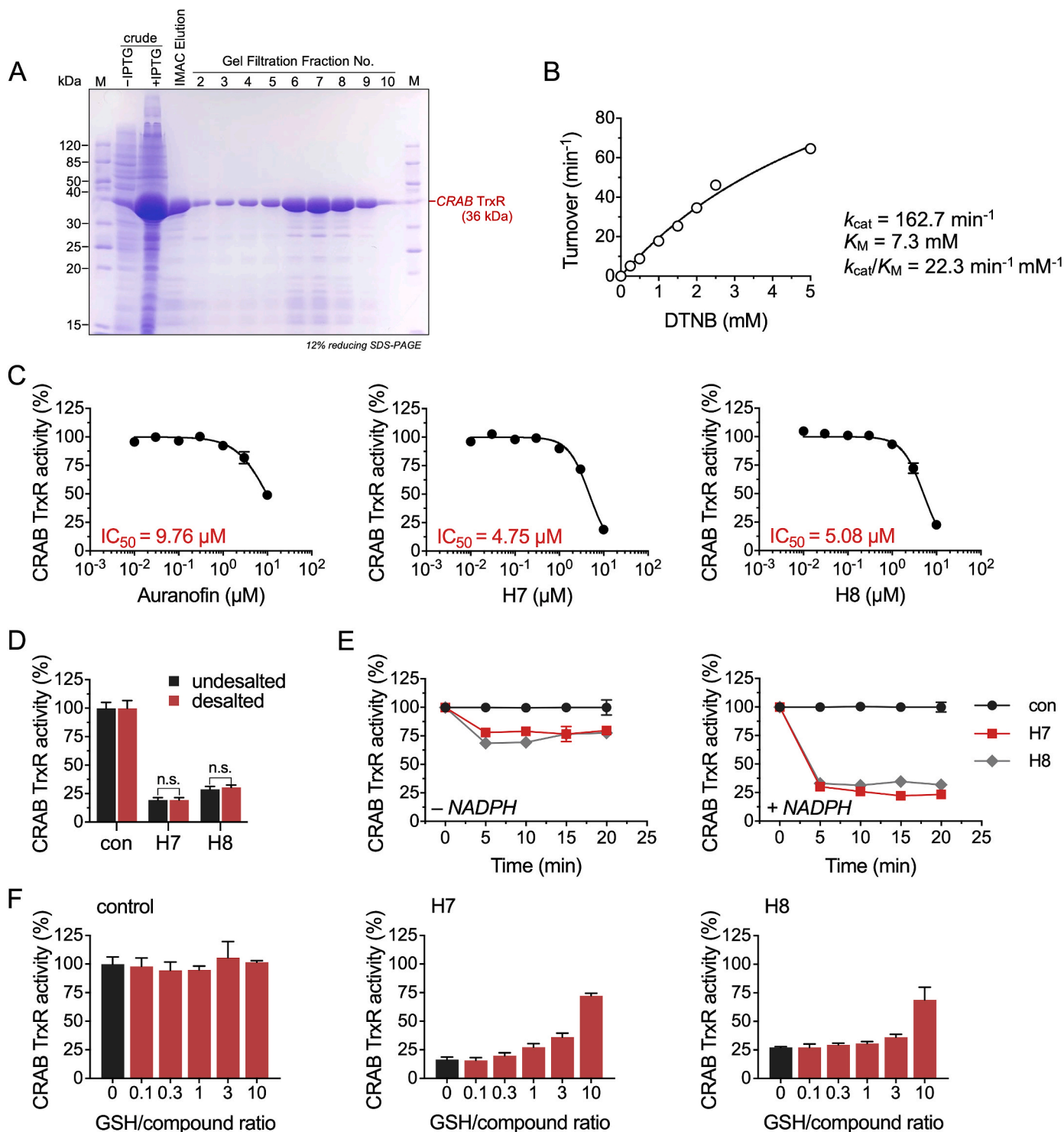


**Fig. 5.** Directly inhibition of recombinant CRAB TrxR by H7 and H8. (A) SDS-PAGE analysis of recombinant CRAB TrxR expressed in *E. coli*. (B) Kinetic parameters for the reduction of DTNB by recombinant CRAB TrxR. (C) Inhibition of recombinant CRAB TrxR by AF, H7, and H8, respectively. (D) Irreversible inhibition of recombinant CRAB TrxR by H7 and H8, separately. (E) NADPH-reduced CRAB TrxR is susceptible to H7 and H8 treatments. (F) Preincubation of GSH separately with H7 and H8 abolishes their inhibitory effects on CRAB TrxR.

and **H8** (Fig. 5D) (Fig. S12A). To investigate the covalent binding sites between **H7**, **H8** and TrxR, TrxR was pre-reduced by NADPH to reduce the redox-active disulfide bond and then incubated with **H7** and **H8** to measure the enzyme activity. The results showed that NADPH-reduced TrxR is susceptible to **H7** and **H8** treatments (Fig. 5E), which indicated that **H7** and **H8** might bind to the redox-active motif. To further confirm this speculation, **H7** and **H8** were separately preincubated with GSH, and NADPH-reduced TrxR was incubated with GSH-conjugated **H7** and **H8** respectively to measure the TrxR activity. The results showed that preincubation of GSH separately with **H7** and **H8** abolishes their inhibitory effects on recombinant CRAB TrxR. These results suggest that **H7** and **H8** have strong sulfhydryl modification ability, therefore, **H7** and **H8** compounds irreversibly inhibited the bacterial TrxR activity by targeting the redox-active motif.

### 3.5. Effect of gold complexes on superoxide radical accumulation in CRAB

The Trx system plays the most powerful regulator to defend against cellular oxidative stress and redox disturbance, while inhibition of TrxR will stimulate the ROS production, perturb the cellular redox homeostasis [39]. Dihydroethidium (DHE) is one of the most commonly used fluorescent probes for detecting superoxide radical, and can be oxidized to form ethyl oxide by intracellular ROS, producing red fluorescence through incorporation into chromosomal DNA [40]. The intensity of red fluorescence is proportional to the level of superoxide radical in cells. Then, CRAB was exposed to different concentrations of auranofin, **H7** and **H8** for 30 min to measure the accumulation of superoxide radical. The results showed that treatment groups had higher red fluorescence than that control group, which indicated that the gold complexes inhibit the activity of TrxR, abolishing the capacity of TrxR to quench superoxide radical and leading to cellular ROS accumulation (Fig. 6a–c). We

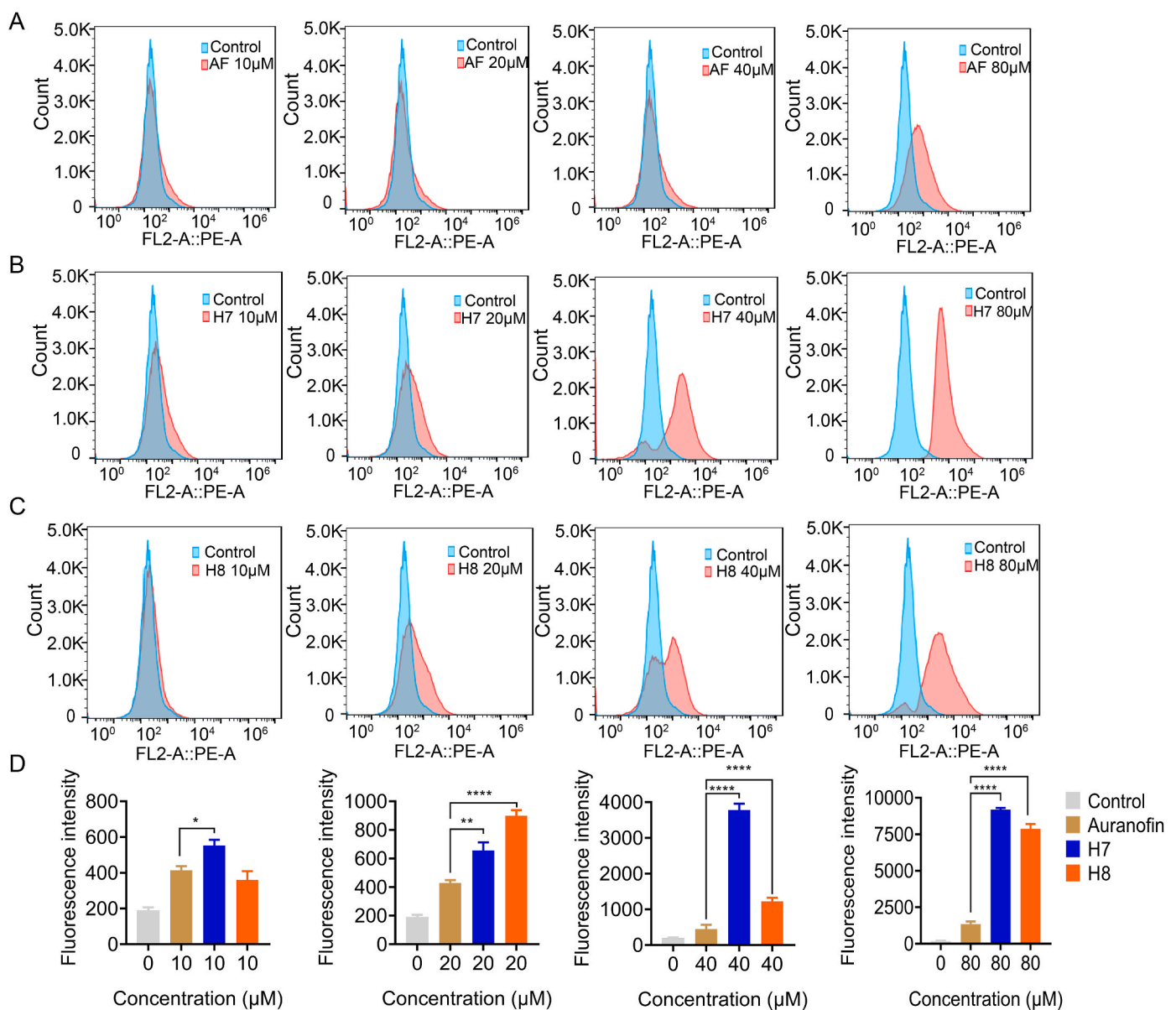


**Fig. 6.** Effect of gold complexes on superoxide radical accumulation. Population heterogeneity of CRAB treated with different concentrations (0, 10, 20, 40, and 80 μM) of auranofin (A), **H7** (B) and **H8** (C) was measured by single-parameter FC analysis of oxidative stress. (D) Total superoxide radical accumulation in CRAB treated with different concentrations (0, 10, 20, 40, and 80 μM) of auranofin, **H7** and **H8**. Statistical significance of the differences in mean values are \* $p < 0.05$ , \*\* $p < 0.01$ , \*\*\* $p < 0.001$ , and \*\*\*\* $p < 0.0001$ . (For interpretation of the references to color in this figure legend, the reader is referred to the Web version of this article.)

observed that the intensity of superoxide radical accumulation in CRAB after treatment with **H7** (10  $\mu\text{M}$ ) was higher than that of auranofin, and both **H7**, **H8** could greatly cause superoxide radical accumulation than that of auranofin when the concentration of the drug is above 20  $\mu\text{M}$  (Fig. 6d). In addition, among the three compounds, the superoxide radical fluorescence intensity caused by **H7** was the highest. Thus, these data suggested that the higher the TrxR affinity of complexes, the more superoxide radicals accumulated.

Previous studies have reported that excessive ROS cause significant damage to a variety of molecules involved in the cell structure, such as lipids, which could increase cell membrane permeability and accelerate cell death [41]. Thus, we used a propidium iodide (PI) probe to measure the effect of gold complexes (auranofin, **H7** and **H8**) on CRAB cell membrane integrity. The results showed that treatment groups had higher red fluorescence than that control group, which indicated that

the gold complexes could increase cell membrane permeability. We observed that the degree of damage to cell membrane integrity increased with an increasing gold complexes (**H7** and **H8**) concentrations, which demonstrated a much stronger effect on cell membrane destruction than auranofin (Fig. 7a–d). Furthermore, the red fluorescence intensity caused by **H7** (40, 80  $\mu\text{M}$ ) was the highest, which indicated that the more ROS accumulated, the severer cell membrane was damaged. In addition, bacterial contents, including some iron ( $\text{K}^+$  and  $\text{Mg}^{2+}$ ), were released in a dose-dependent manner by **H7** and **H8** (Fig. S13), confirming that the cell membrane structure was destroyed.

### 3.6. Killing mechanism of complexes **H7** and **H8**

Compared with auranofin, **H7** and **H8** showed certain advantages and the killing mechanism of **H7** and **H8** deserves further study.

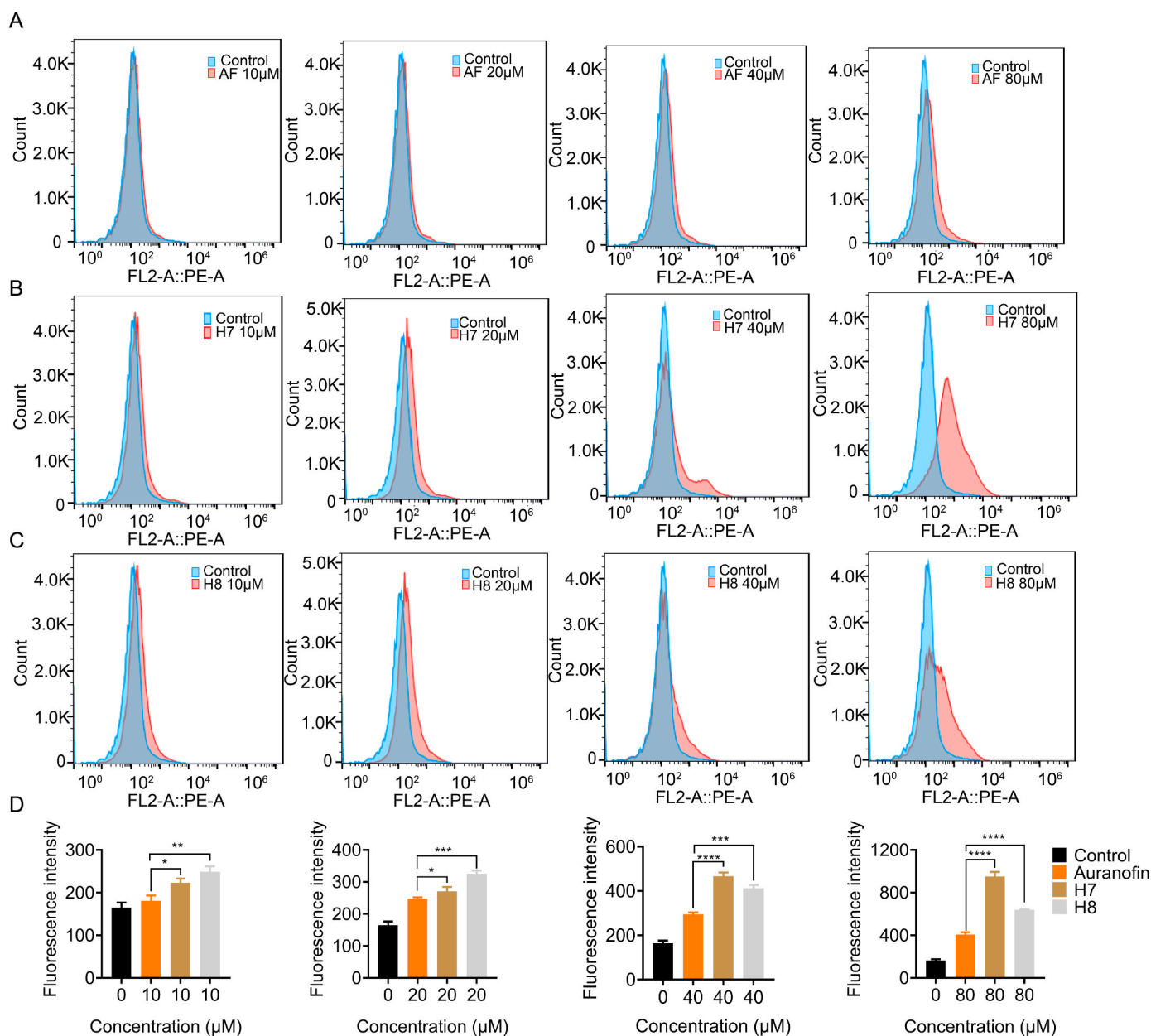


**Fig. 7.** Effect of gold complexes on membrane integrity. Population heterogeneity of CRAB treated with different concentrations (0, 10, 20, 40, and 80  $\mu\text{M}$ ) of Auranofin (A), **H7** (B) and **H8** (C) were measured by single-parameter FC analysis of membrane integrity. (D) The intensity of red fluorescence in CRAB treated with different concentrations (0, 10, 20, 40, and 80  $\mu\text{M}$ ) of auranofin, **H7** and **H8**. Statistical significance of the differences in mean values are \* $p < 0.05$ , \*\* $p < 0.01$ , \*\*\* $p < 0.001$ , and \*\*\*\* $p < 0.0001$ . (For interpretation of the references to color in this figure legend, the reader is referred to the Web version of this article.)



DNA, membrane lipids and proteins. It has been reported that ROS can cause protein inactivation and destabilization through covalent modifications [43]. For example, arginine, lysine, proline, etc. can be modified to oxo-histidine, and some amino acids containing electron-rich sulfur atoms, such as cysteine, would be particularly sensitive to oxidation [44,45]. Thus, our results further indicated that the metabolism of amino acids in the cell was disrupted due to cellular superoxide radical accumulation.

However, a small but essential metabolite of the pentose phosphate pathway (PPP) showed higher abundance after treatment with **H7** and **H8** (Fig. 9). When exposed to stress conditions, mammalian cells employ metabolic reprogramming in the short term. For example, NADPH plays a vitally important role in alleviating oxidative stress; [46] upon exposure to ROS, cells reroute glucose metabolism through the oxidative arm of the PPP to increase the production of NADPH [47]. Our results revealed that there is a consistent feedback mechanism by increasing flux through the oxidative PPP in the bacteria after treatment with **H7** and **H8**, which helps to protect the bacteria from impaired redox homeostasis and damage induced by oxidative stress. Thus, further study of the novel ligands in the gold complex is essential to help disrupt this feedback mechanism.

Aerobic organisms have evolved antioxidant systems to counteract oxidative stress, and enhanced accumulation of the endogenous ROS could impair bacterial antioxidant systems [48]. To understand the antibacterial mechanisms of **H7** and **H8**, we measured the cellular activity levels of GSH, MDA and SOD activity and assessed the effects of oxidative stress induced by complexes **H7** and **H8**. Results showed that both **H7** and **H8** (10, 20, 40  $\mu$ M) significantly decrease the GSH content compared with the control group ( $p < 0.001$ ) (Fig. 10a). What's more, **H7** and **H8** at 10, 20, 40  $\mu$ M significantly increase the MDA content compared with the control group ( $p < 0.05$  or  $p < 0.001$ ) (Fig. 10b). **H7** and **H8** at 10, 20, 40  $\mu$ M significantly suppressed SOD activity compared

with the control group ( $p < 0.01$  or  $p < 0.001$ ) (Fig. 10c). These results showed that **H7** and **H8** could increase the superoxide radical accumulation and MDA levels, but decrease GSH levels and SOD activity in a dose-dependent manner. In addition, DNA degradation was obviously triggered upon treatment with different concentrations of **H7** and **H8** (Fig. 10d). Collectively, the antibacterial mechanisms of **H7** and **H8** were assessed.

Collectively, **H7** and **H8** compounds can irreversibly inhibit the bacterial TrxR activity by targeting the redox-active motif, abolishing the capacity of TrxR to quench superoxide radical and finally leading to oxidative stress. Superoxide radicals impact a variety of functions necessary for bacterial survival, such as cellular redox balance, cell membrane integrity, amino acid metabolism, and lipid peroxidation. In addition, **H7** and **H8** could directly degrade DNA *in vitro*. Such activities likely account for the high efficacy of **H7** and **H8** against CRAB through multiple target pathways.

### 3.7. Reduced infection and promoted wound healing *in vivo*

To explore the *in vivo* effect of gold complexes against CRAB, we assessed the healing effect of **H7**, **H8** and auranofin in an infected wound animal model. A 1.2 cm  $\times$  1.2 cm wound was surgically cut on the backs of BALB/c male mice and then injected with bacterial fluid to establish a skin-infected wound model. When the infection time reached 24 h, these mice were randomly divided into the following five groups ( $n = 4$ ): control group, the infected wound was covered with 30  $\mu$ L of 0.9% NaCl;  $H_2O_2$  group, the infected wound was covered with 30  $\mu$ L of  $H_2O_2$  (5 mM); auranofin group, the infected wound was covered with 30  $\mu$ L of auranofin (5 mM); imipenem group, the infected wound was covered with 30  $\mu$ L of imipenem (5 mM); colistin group, the infected wound was covered with 30  $\mu$ L of colistin (5 mM); **H7** group, the infected wound was covered with 30  $\mu$ L of **H7** (5 mM); and **H8** group, the infected

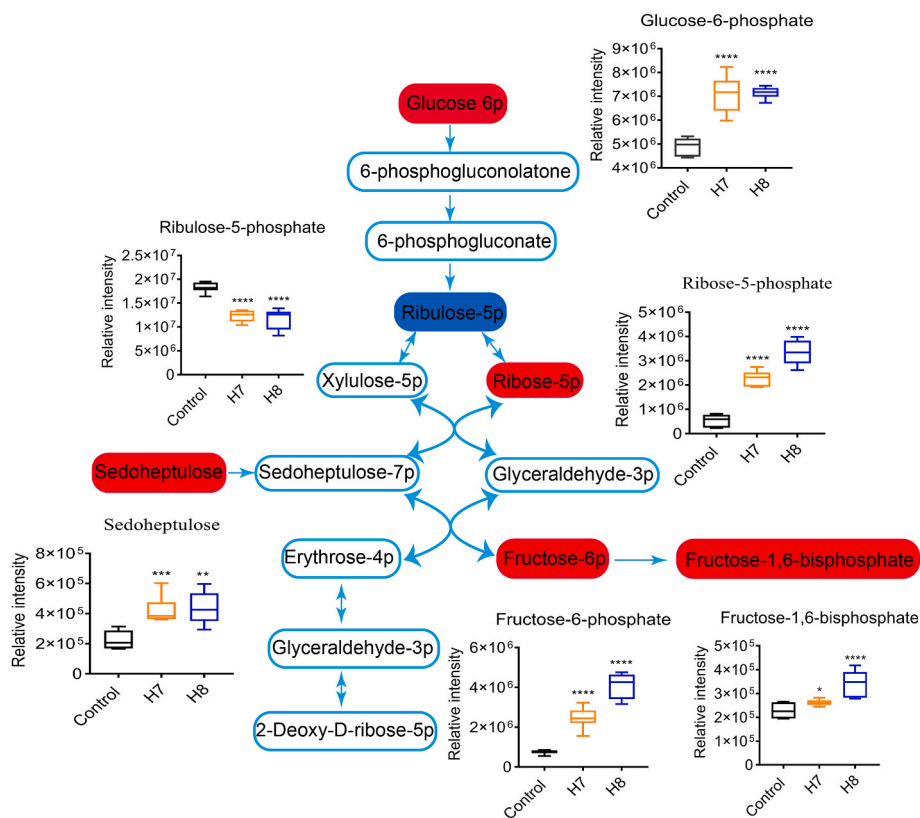


**Fig. 9.** Metabolic changes in the pentose phosphate pathway (PPP) after treatment with **H7** and **H8**. Blue, significant decrease; red, significant increase; blank box, not detected. Statistical significance of the differences in mean values are \* $p < 0.05$ , \*\* $p < 0.01$ , \*\*\* $p < 0.001$ , and \*\*\*\* $p < 0.0001$ . (For interpretation of the references to color in this figure legend, the reader is referred to the Web version of this article.)

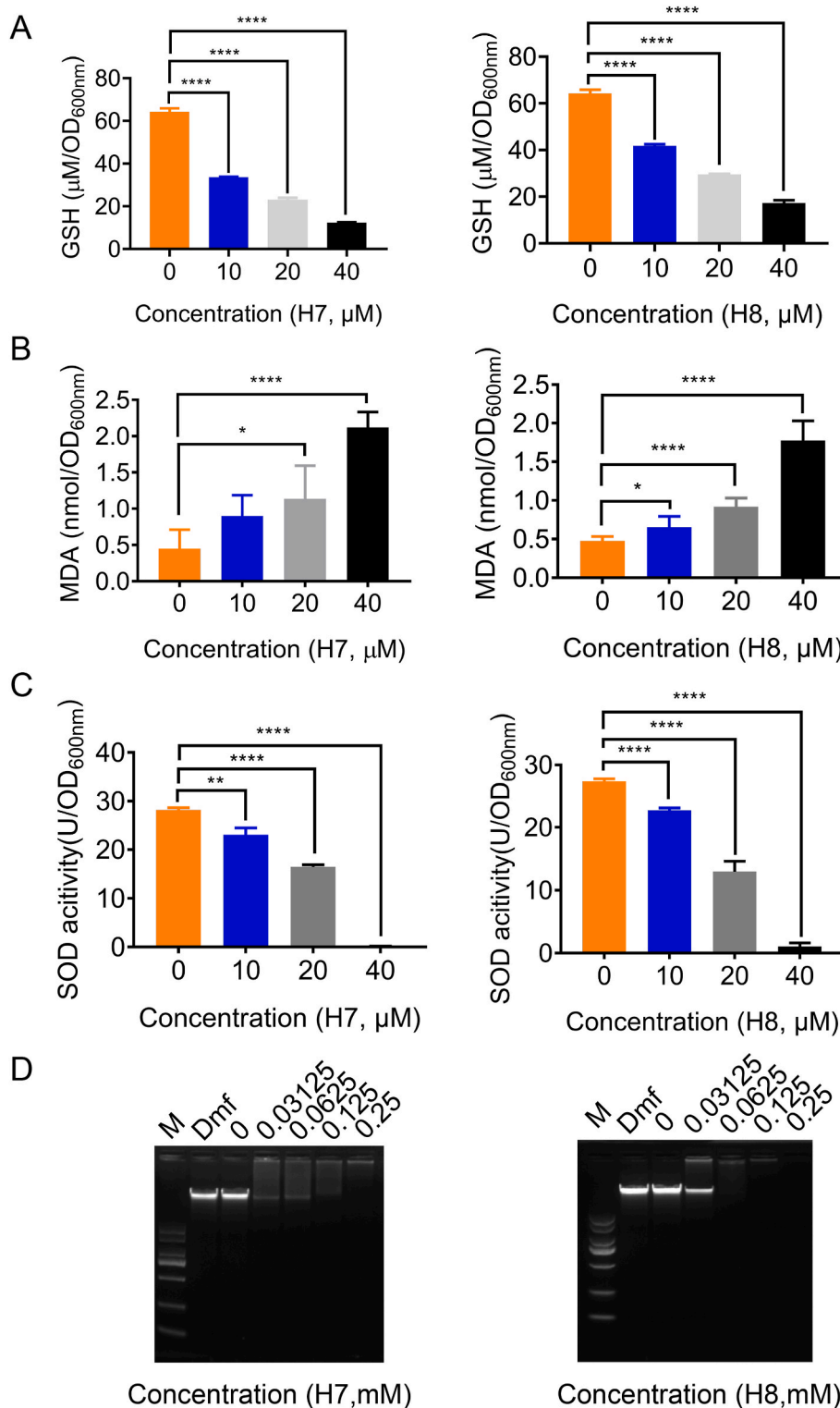


**Fig. 10.** Killing mechanism of **H7** and **H8**. (A) GSH contents of CRAB treated with different concentrations of **H7** and **H8** for 2 h. (B) Lipid peroxidation of CRAB treated with different concentrations of **H7** and **H8** for 2 h. (C) Level of SOD activity of CRAB treated with different concentrations of **H7** and **H8** for 2 h. (D) Genomic DNA degradation of CRAB treated with **H7**, **H8**. M: Marker; DMF: organic solvent; 0: control group. Statistical significance of the differences in mean values are \* $p < 0.05$ , \*\* $p < 0.01$ , \*\*\* $p < 0.001$ , and \*\*\*\* $p < 0.0001$ .

wound was covered with 30 μL of **H8** (5 mM). As shown in Fig. 11a, both the **H7** and **H8** groups showed significant outcomes compared with the control, H<sub>2</sub>O<sub>2</sub>, imipenem, colistin and auranofin groups. None of the body weights of the wound-infected mice were significantly different (Fig. 11c). The wounds showed remarkable healing and size reduction after **H7** and **H8** treatment, which exhibited better effects than auranofin, imipenem and colistin treatment at the same dose (Fig. 11d). In addition, HE staining analysis further confirmed that inflammation subsided in the **H7** and **H8** groups (Fig. 11b). The results of

immunohistochemical analysis showed that the expression of proinflammation-related genes was also significantly downregulated by **H7** and **H8** treatment (Fig. 11b). Together, our data demonstrated that treatment with **H7** and **H8** presented better antibacterial activity than treatment with auranofin, imipenem and colistin reduced infection and promoted wound healing.

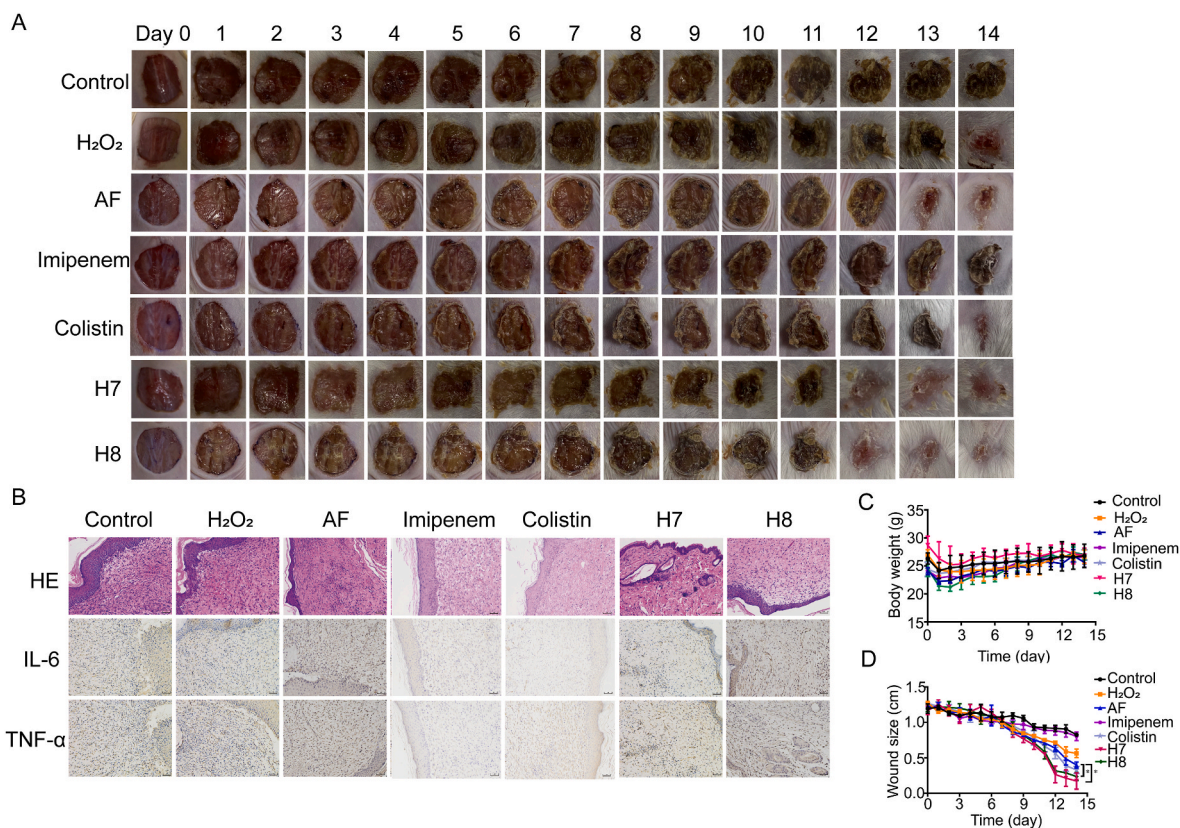


**Fig. 11.** H7 and H8 reduce infection and promote wound healing. (A) Photographs of CRAB-infected wounds on mice treated with 0.9% (m/v) NaCl (control group), H<sub>2</sub>O<sub>2</sub>, auranofin, imipenem, colistin, H7 and H8 (n = 4). (B) HE staining and immunohistochemistry of inflammatory markers (IL-6 and TNF- $\alpha$ ) in infected wounds from each group on Day 14. (C) and (D) Illustration of the body weights and wound size change during treatments. Statistical significance of differences in the mean values are \*p < 0.050.

### 3.8. Effective prolongation of the survival time of CRAB-induced peritonitis

In this experiment, we evaluated the antibacterial ability of H7 and H8 to protect mice from CRAB-induced peritonitis. BALB/c male mice were infected i.p. with bacterial fluid (200  $\mu$ L  $1 \times 10^9$  cfu/mL) of CRAB to establish a model of abdominal infection. At 1 h after infection, all of the mice were randomly divided into 4 groups (n = 8): control group, mice were treated with a single i.p. injection of PBS; auranofin group, mice were treated with a single i.p. injection of auranofin (5 mg/kg); H7 group, mice were treated with a single i.p. injection of H7 (5 mg/kg); H8 group, mice were treated with a single i.p. injection of H8 (5 mg/kg). Treatment was given only 1 h after infection, and survival within 72 h was observed. The results showed that none of the mice in the control group survived beyond 12 h; four of the eight mice treated with auranofin survived to 24 h; three of the eight mice treated with H7 survived longer to 48 h; and two of the eight mice treated with H8 survived up to 72 h (Fig. 12).

As comparison, we performed the same experiment in female mice, and the results showed that none of the mice in the control group survived beyond 26 h; seven of the twelve mice treated with auranofin survived to 34 h; three of the twelve mice treated with H7 survived to 55 h, and two of the twelve mice treated with H7 survived up to 72 h; and six of the twelve mice treated with H8 survived to 55 h, and three of the twelve mice treated with H8 survived up to 72 h (Fig. S16). These results suggest that treatments with H7 and H8 remarkably present much better antibacterial activity *in vivo* than auranofin and greatly prolong the survival time.

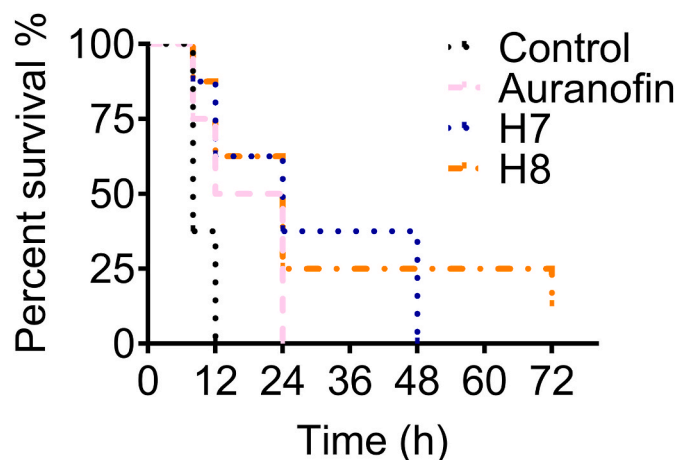


**Fig. 12.** H7 and H8 prolong the survival time of the CRAB-induced peritonitis model. BALB/c mice were infected i.p. with bacterial fluid to establish a model of abdominal infection. Treatment was given only 1 h after infection, and survival within 72 h was observed.

## 4. Conclusions

In summary, the results of antibacterial activity demonstrate that a series of gold(I) selenium NHC complexes, particularly H7 and H8, exhibited marked potency antibacterial activity against MDR bacteria than the FDA-approved gold(I) drug (auranofin). The antibacterial mechanisms of these two gold(I) complexes were related to cellular DNA degradation and irreversible inhibition of the bacterial TrxR via

targeting the redox-active motif. Upon treatment of **H7** and **H8**, the capacity of bacterial TrxR to quench ROS was abolished, leading to oxidative stress, and further cellular metabolic dysfunction. Noteworthy, **H7** and **H8** present significant antibacterial activity in vivo compared to auranofin, remarkably reduced infections and profoundly promoted wound healing in mouse models, and effectively prolonged the survival time of CRAB-induced peritonitis. Thus, both complexes **H7** and **H8** have represented great potential as drug candidates for the treatment of MDR bacteria.

#### Declaration of competing interest

The authors declare no competing financial interest.

#### Acknowledgments

We thank the financial supports of the National Natural Science Foundation of China (No. 82173684, 82073913), the Open Project of Chinese Materia Medical First-Class Discipline of Nanjing University of Chinese Medicine (No. 2020YLXK010), the Priority Academic Program Development of Jiangsu Higher Education Institutions (Integration of Chinese and Western Medicine), the Natural Science Foundation of the Jiangsu Higher Education Institutions of China (No. 22KJB310002). We thank for the experimental support from the Experiment Center for Science and Technology, Nanjing University of Chinese Medicine, China. The research is also financially supported by the “Innovative and Entrepreneurial Team” Program of Jiangsu Province (2020). And our team is led by Prof. Ming Zhao, Nanjing University of Chinese Medicine.

#### Appendix A. Supplementary data

Supplementary data to this article can be found online at <https://doi.org/10.1016/j.redox.2023.102621>.

#### Abbreviations used

MDR	Multidrug-resistant
CRE	carbapenem-resistant <i>Enterobacteriaceae</i>
ROS	reactive oxygen species
TrxR	thioredoxin reductase
CRAB	carbapenem-resistant <i>Acinetobacter baumannii</i>
CRPA	carbapenem-resistant <i>Pseudomonas aeruginosa</i>
CRKP	carbapenem-resistant <i>Klebsiella pneumoniae</i>
CREco	carbapenem-resistant <i>Escherichia coli</i>
WHO	World Health Organization
Trx	Thioredoxin
MBLs	metallo- $\beta$ -lactamases
Se	selenium
NHCs	N-heterocyclic carbenes
CCK-8	Cell Counting Kit-8
KotBu	potassium <i>tert</i> -butoxide
FICI	fractional inhibitory concentration index
THF	tetrahydrofuran
VISA	vancomycin-intermediate <i>Staphylococcus aureus</i>
DHE	Dihydroethidium
PI	propidium iodide
PPP	pentose phosphate pathway
MDA	malondialdehyde
SOD	superoxide dismutase
Grx	glutaredoxin
GSH	glutathione

#### References

- [1] Y. Doi, Treatment options for carbapenem-resistant gram-negative bacterial infections, *Clin. Infect. Dis.* 69 (2019) S565–S575.
- [2] B.N. Dang, D.Y. Graham, *Helicobacter pylori* infection and antibiotic resistance: a WHO high priority? *Nat. Rev. Gastroenterol. Hepatol.* 14 (2017) 383–384.
- [3] Y. Zhang, Q. Wang, Y. Yin, H. Chen, L. Jin, B. Gu, L. Xie, C. Yang, X. Ma, H. Li, W. Li, X. Zhang, K. Liao, S. Man, S. Wang, H. Wen, B. Li, Z. Guo, J. Tian, F. Pei, L. Liu, L. Zhang, C. Zou, T. Hu, J. Cai, H. Yang, J. Huang, X. Jia, W. Huang, B. Cao, H. Wang, Epidemiology of carbapenem-resistant *Enterobacteriaceae* infections: report from the China CRE network, *Antimicrob. Agents Chemother.* 62 (2018).
- [4] S.M. Bartsch, J.A. McKinnell, L.E. Mueller, L.G. Miller, S.K. Gohil, S.S. Huang, B. Y. Lee, Potential economic burden of carbapenem-resistant *Enterobacteriaceae* (CRE) in the United States, *Clin. Microbiol. Infect.* 23 (2017).
- [5] U. Theuretzbacher, K. Bush, S. Harbarth, M. Paul, J.H. Rex, E. Tacconelli, G. E. Thwaites, Critical analysis of antibacterial agents in clinical development, *Nat. Rev. Microbiol.* 18 (2020) 286–298.
- [6] J.H. Rex, H. Fernandez Lynch, I.G. Cohen, J.J. Darrow, K. Outtersson, Designing development programs for non-traditional antibacterial agents, *Nat. Commun.* 10 (2019) 3416.
- [7] X. Ren, L. Zou, A. Holmgren, Targeting bacterial antioxidant systems for antibiotics development, *Curr. Med. Chem.* 27 (2020) 1922–1939.
- [8] J. Lu, A. Holmgren, The thioredoxin antioxidant system, *Free Radic. Biol. Med.* 66 (2014) 75–87.
- [9] X. Liao, F. Yang, H. Li, P.-K. So, Z. Yao, W. Xia, H. Sun, Targeting the thioredoxin reductase-thioredoxin system from *Staphylococcus aureus* by silver ions, *Inorg. Chem.* 56 (2017) 14823–14830.
- [10] X. Ren, L. Zou, J. Lu, A. Holmgren, Selenocysteine in mammalian thioredoxin reductase and application of ebselen as a therapeutic, *Free Radic. Biol. Med.* 127 (2018) 238–247.
- [11] J.-J. Zhang, M.A. Abu El Maaty, H. Hoffmeister, C. Schmidt, J.K. Muenzner, R. Schobert, S. Wölfel, I. Ott, A multitarget gold(I) complex induces cytotoxicity related to aneuploidy in HCT-116 colorectal carcinoma cells, *Angew. Chem. Int. Ed. Engl.* 59 (2020) 16795–16800.
- [12] Y. Long, B. Cao, X. Xiong, A.S.C. Chan, R.W.-Y. Sun, T. Zou, Bioorthogonal activation of dual catalytic and anti-cancer activities of organogold(I) complexes in living systems, *Angew. Chem. Int. Ed. Engl.* 60 (2021) 4133–4141.
- [13] F. Paladini, M. Pollini, A. Sannino, L. Ambrosio, Metal-based antibacterial substrates for biomedical applications, *Biomacromolecules* 16 (2015) 1873–1885.
- [14] E.K. Dennis, J.H. Kim, S. Parkin, S.G. Awuah, S. Garneau-Tsodikova, Distorted gold (I)-Phosphine complexes as antifungal agents, *J. Med. Chem.* 63 (2020) 2455–2469.
- [15] M.B. Harbut, C. Vilchèze, X. Luo, M.E. Hensler, H. Guo, B. Yang, A.K. Chatterjee, V. Nizet, W.R. Jacobs, P.G. Schultz, F. Wang, Auranofin exerts broad-spectrum bactericidal activities by targeting thiol-redox homeostasis, *Proc. Natl. Acad. Sci. U. S. A.* 112 (2015) 4453–4458.
- [16] H. Sun, Q. Zhang, R. Wang, H. Wang, Y.-T. Wong, M. Wang, Q. Hao, A. Yan, R.Y.-T. Kao, P.-L. Ho, H. Li, Resensitizing carbapenem- and colistin-resistant bacteria to antibiotics using auranofin, *Nat. Commun.* 11 (2020) 5263.
- [17] Y. Liu, Y. Lu, Z. Xu, X. Ma, X. Chen, W. Liu, Repurposing of the gold drug auranofin and a review of its derivatives as antibacterial therapeutics, *Drug Discov. Today* 27 (2022) 1961–1973.
- [18] B. Wu, X. Yang, M. Yan, Synthesis and structure-activity relationship study of antimicrobial auranofin against ESKAPE pathogens, *J. Med. Chem.* 62 (2019) 7751–7768.
- [19] T. Zou, C.T. Lum, C.-N. Lok, J.-J. Zhang, C.-M. Che, Chemical biology of anticancer gold(III) and gold(I) complexes, *Chem. Soc. Rev.* 44 (2015) 8786–8801.
- [20] Y. Pang, B. An, L. Lou, J. Zhang, J. Yan, L. Huang, X. Li, S. Yin, Design, synthesis, and biological evaluation of novel selenium-containing isocombretastatin and phenstatins as antitumor agents, *J. Med. Chem.* 60 (2017) 7300–7314.
- [21] W. Liu, R. Gust, Metal N-heterocyclic carbene complexes as potential antitumor metallodrugs, *Chem. Soc. Rev.* 42 (2013) 755–773.
- [22] Y. Li, G.-F. Liu, C.-P. Tan, L.-N. Ji, Z.-W. Mao, Antitumor properties and mechanisms of mitochondria-targeted Ag(I) and Au(I) complexes containing N-heterocyclic carbenes derived from cyclophanes, *Metallomics* 6 (2014) 1460–1468.
- [23] R. Fan, M. Bian, L. Hu, W. Liu, A new rhodium(I) NHC complex inhibits TrxR: in vitro cytotoxicity and in vivo hepatocellular carcinoma suppression, *Eur. J. Med. Chem.* 183 (2019), 111721.
- [24] W. Liu, K. Benschdorf, M. Proetto, U. Abram, A. Hagenbach, R. Gust, NHC gold halide complexes derived from 4,5-diarylimidazoles: synthesis, structural analysis, and pharmacological investigations as potential antitumor agents, *J. Med. Chem.* 54 (2011) 8605–8615.
- [25] J.R. Stenger-Smith, P.K. Mascharak, Gold drugs with {Au(PPh<sub>3</sub>)<sub>3</sub>} moiety: advantages and medicinal applications, *ChemMedChem* 15 (2020) 2136–2145.
- [26] A.M. Bobenchik, E. Deak, J.A. Hindler, C.L. Charlton, R.M. Humphries, Performance of vitek 2 for antimicrobial susceptibility testing of *acinetobacter baumannii*, *Pseudomonas aeruginosa*, and *stentrophomonas maltophilia* with vitek 2 (2009 FDA) and CLSI M100S 26th edition breakpoints, *J. Clin. Microbiol.* 55 (2017) 450–456.
- [27] B. Yuan, P. Wang, L. Sang, J. Gong, Y. Pan, Y. Hu, QNAR modeling of cytotoxicity of mixing nano-TiO and heavy metals, *Ecotoxicol. Environ. Saf.* 208 (2021), 111634.
- [28] M. Bian, R. Fan, G. Jiang, Y. Wang, Y. Lu, W. Liu, Halo and pseudohalo gold(I)-NHC complexes derived from 4,5-diarylimidazoles with excellent and anticancer activities against HCC, *J. Med. Chem.* 63 (2020) 9197–9211.

- [29] J. Xu, V. Croitoru, D. Rutishauser, Q. Cheng, E.S.J. Arnér, Wobble decoding by the *Escherichia coli* selenocysteine insertion machinery, *Nucleic Acids Res.* 41 (2013) 9800–9811.
- [30] S. Sun, W. Xu, H. Zhou, Y. Zhang, J. Zhang, X. Li, B. Li, K. Ma, J. Xu, Efficient purification of selenoprotein thioredoxin reductase 1 by using chelating reagents to protect the affinity resins and rescue the enzyme activities, *Process Biochem.* 101 (2021) 256–265.
- [31] S. Sun, W. Xu, Y. Zhang, Y. Yang, Q. Ma, J. Xu, Menadione inhibits thioredoxin reductase 1 via arylation at the Sec residue and enhances both NADPH oxidation and superoxide production in Sec to Cys substitution, *Free Radic. Biol. Med.* 172 (2021) 482–489.
- [32] Y. Zhang, S. Sun, W. Xu, R. Yang, Y. Yang, J. Guo, K. Ma, J. Xu, Thioredoxin reductase 1 inhibitor shikonin promotes cell necroptosis via SecTRAPs generation and oxygen-coupled redox cycling, *Free Radic. Biol. Med.* 180 (2022) 52–62.
- [33] M.H.M. Maifiah, D.J. Creek, R.L. Nation, A. Forrest, B.T. Tsuji, T. Velkov, J. Li, Untargeted metabolomics analysis reveals key pathways responsible for the synergistic killing of colistin and doripenem combination against *Acinetobacter baumannii*, *Sci. Rep.* 7 (2017), 45527.
- [34] J.-L. Tao, Y.-Z. Chen, Q.-G. Dai, M. Tian, S.-C. Wang, J.-J. Shan, J.-J. Ji, L.-L. Lin, W.-W. Li, B. Yuan, Urine metabolic profiles in paediatric asthma, *Respirology* 24 (2019) 572–581.
- [35] S. Huang, X. Sheng, M. Bian, Z. Yang, Y. Lu, W. Liu, Synthesis and in vitro anticancer activities of selenium N-heterocyclic carbene compounds, *Chem. Biol. Drug Des.* 98 (2021) 435–444.
- [36] J. Jampilek, Design and discovery of new antibacterial agents: advances, perspectives, challenges, *Curr. Med. Chem.* 25 (2018) 4972–5006.
- [37] L. Felix, E. Mylonakis, B.B. Fuchs, Thioredoxin reductase is a valid target for antimicrobial therapeutic development against gram-positive bacteria, *Front. Microbiol.* 12 (2021), 663481.
- [38] M. Bian, Y. Sun, Y. Liu, Z. Xu, R. Fan, Z. Liu, W. Liu, A gold(I) complex containing an oleanolic acid derivative as a potential anti-ovarian-cancer agent by inhibiting TrxR and activating ROS-mediated ERS, *Chemistry* 26 (2020) 7092–7108.
- [39] H. Zou, J. Zhang, C. Wu, B. He, Y. Hu, H.H.Y. Sung, R.T.K. Kwok, J.W.Y. Lam, L. Zheng, B.Z. Tang, Making aggregation-induced emission luminogen more valuable by gold: enhancing anticancer efficacy by suppressing thioredoxin reductase activity, *ACS Nano* 15 (2021) 9176–9185.
- [40] J. Song, X. Gao, Z. Tang, H. Li, Y. Ruan, Z. Liu, T. Wang, S. Wang, J. Liu, H. Jiang, Protective effect of Berberine on reproductive function and spermatogenesis in diabetic rats via inhibition of ROS/JAK2/NFκB pathway, *Andrology* 8 (2020) 793–806.
- [41] S.S. Seyedjavadi, S. Khani, A. Eslamifar, S. Ajdary, M. Goudarzi, R. Halabian, R. Akbari, H. Zare-Zardini, A.A. Imani Fooladi, J. Amani, M. Razzaghi-Abyaneh, The antifungal peptide MCh-AMP1 derived from inhibits growth via inducing ROS generation and altering fungal cell membrane permeability, *Front. Microbiol.* 10 (2019) 3150.
- [42] C.H. Johnson, J. Ivanisevic, G. Siuzdak, Metabolomics: beyond biomarkers and towards mechanisms, *Nat. Rev. Mol. Cell Biol.* 17 (2016) 451–459.
- [43] B. Ezraty, A. Gennaris, F. Barras, J.-F. Collet, Oxidative stress, protein damage and repair in bacteria, *Nat. Rev. Microbiol.* 15 (2017) 385–396.
- [44] T. Nyström, Role of oxidative carbonylation in protein quality control and senescence, *EMBO J.* 24 (2005) 1311–1317.
- [45] D.A.K. Traoré, A. El Ghazouani, L. Jacquamet, F. Borel, J.-L. Ferrer, D. Lascoux, J.-L. Ravanat, M. Jaquinod, G. Blondin, C. Caux-Thang, V. Duarte, J.-M. Latour, Structural and functional characterization of 2-oxo-histidine in oxidized PerR protein, *Nat. Chem. Biol.* 5 (2009) 53–59.
- [46] J.D. Hayes, A.T. Dinkova-Kostova, K.D. Tew, Oxidative stress in cancer, *Cancer Cell* 38 (2020) 167–197.
- [47] A. Kuehne, H. Emmert, J. Soehle, M. Winnefeld, F. Fischer, H. Wenck, S. Gallinat, L. Terstegen, R. Lucius, J. Hildebrand, N. Zamboni, Acute activation of oxidative pentose phosphate pathway as first-line response to oxidative stress in human skin cells, *Mol. Cell* 59 (2015) 359–371.
- [48] A.T. Dharmaraja, Role of reactive oxygen species (ROS) in therapeutics and drug resistance in cancer and bacteria, *J. Med. Chem.* 60 (2017) 3221–3240.